EXTRACTION OF NONLINEAR INDICIAL AND CRITICAL STATE RESPONSES FROM EXPERIMENTAL DATA

Patrick H. Reisenthel[‡] and Matthew T. Bettencourt[¶]
Nielsen Engineering & Research, Inc.
Mountain View, CA

ABSTRACT

Practical application of nonlinear indicial theory is of interest for the rapid, yet high-fidelity, modeling of unsteady aerodynamic phenomena. The present paper addresses the question of how to extract nonlinear indicial and critical-state responses from empirical data which were not specifically designed for this purpose. The extraction algorithm is presented, and the results are illustrated on the case of the rolling moment response of a 65-degree delta wing undergoing forced roll oscillations.

NOMENCLATURE

Symbols and abbreviations

b	Wing span
c	Wing chord
C_l	Rolling moment coefficient
CS	Critical State
CSR	Critical State Response
f	Aerodynamic load (generic)
f	Frequency
f_ϕ	Indicial response of f with respect to ϕ
$\tilde{f}$	Indicial response of f
$\tilde{h}$	Deficiency function ($\tilde{h} \equiv \tilde{f}(t) - \tilde{f}(t \to \infty)$)
H	Heaviside step function
IE	Indicial Extraction
IP	Indicial Prediction
IPS	Indicial Prediction System
IR	Indicial Response
k	Reduced frequency ($k \equiv \omega b/2U_\infty$)
n_{harm}	Number of retained harmonics
N_ϕ	Number of nodal extraction roll angles
p	Roll rate
QS	Quasi-static
sgn	Sign
SMS	Stochastic Matrix Solving
SVD	Singular Value Decomposition
t	Time
T	Period of oscillation
U_∞	Freestream velocity
α	Angle of attack
δ	Dirac delta function
$\delta C_l/\delta\phi$	Indicial response of rolling moment with respect to roll angle
Δf	Build-up of generic aerodynamic load, f
Δf^{CS}	Critical-state response of f
ϵ	Boundary condition (generic)
ϕ	Roll angle
τ	Auxiliary time variable
τ_c	Time at which critical state is crossed
ω	Angular frequency
ξ	Parameter denoting dependence on prior motion history
$\xi_j(t)$	Basis function

Subscripts

c	Critical
CS	Critical State
DR	Deficiency Response
dyn	Dynamic
QS	Quasi-static
∞	Time-asymptotic value (except for U_∞)

Superscripts

CS	Critical State
dyn	Dynamic component
v	Vortical
$\bullet$	Derivative with respect to time
$\bullet\bullet$	Second derivative with respect to time
$\sim$	Indicial or deficiency function

[‡] Chief Scientist, Member AIAA
[¶] Research Scientist. Presently at University of Southern Mississipi.

1. PROBLEM DEFINITION AND OBJECTIVE

In order to predict the dynamics of maneuvering aircraft or missiles at high angles of attack, it is essential to accurately and efficiently model the nonlinearities associated with post-stall aerodynamics, including bifurcations and hysteresis. It has been shown (Refs. 1-3) that a possible solution to these modeling requirements is to make use of nonlinear indicial theory (Refs. 4,5).

The overall objective of this work was the development of an aerodynamic prediction capability based on nonlinear indicial response theory. The results of earlier studies (Refs. 6-8) had demonstrated the feasibility of building such a model using key simplifications based on the original formulation proposed by Tobak et al. (Ref. 4) and Tobak and Chapman (Ref. 5). Indicial-theoretical models are, by nature, *constructive*: they attempt to predict the time-dependent output(s) of a nonlinear "system" based on the knowledge of the system's kernel of indicial and critical-state responses. The identification of this response kernel is, therefore, a critical element of any indicial prediction method.

The present paper describes a new method allowing the extraction of indicial and critical-state responses from experimental data of a fairly general nature. This paper is organized as follows. First, a brief theoretical background is given. This is followed by a description of the extraction algorithm. Finally, validation examples are provided, including a demonstration of the method for the case of the rolling moment response of a 65-degree delta wing at high angle of attack. A more detailed description of the 65-degree delta wing nonlinear indicial response model is also given in a companion paper, Ref. 9.

2. INDICIAL THEORY

The indicial approach is based on the concept that a variable $f(t)$, which describes the state of the flow, can be linearized with respect to its boundary condition (or forcing function), $\epsilon(t)$, if the variation of $f(t)$ is a smooth function of $\epsilon(t)$. This allows the representation of $f(t)$ in a Taylor series about some value of $\epsilon = \epsilon_0$; thus

$$f(t) = f(0) + \Delta\epsilon \left.\frac{\partial f}{\partial\epsilon}\right|_{\epsilon=\epsilon_0} + \cdots$$

If the response $\partial f/\partial\epsilon$ depends only on the elapsed time from the perturbation $\Delta\epsilon$ (a linear time invariant response), then it may be shown (Ref. 10) that the formal solution for $f(t)$ is

$$f(t) = \tilde{f}(t)\epsilon(0) + \int_0^t \frac{d\epsilon}{d\tau}\tilde{f}(t-\tau)d\tau \qquad (1)$$

where $\tilde{f}(t) = \left.\dfrac{\partial f}{\partial\epsilon}\right|_{\epsilon=\epsilon_0}$.

Hence, if the forcing function (i.e., the boundary condition ϵ) is known and if $\tilde{f}$ (the indicial response) is known from some computation or experiment, then **Eq. (1)** gives the value of $f(t)$ for any schedule of the boundary condition $\epsilon(t)$ without the need to compute f from first principles.

The basic idea behind the use of *nonlinear* indicial response theory (Refs. 4,5) is that the linear formalism, **Eq. (1)**, can be retained in the form of a generalized superposition integral, provided that the nonlinear indicial response $\tilde{f}$ is now taken to be a functional $\tilde{f}(\epsilon(\xi);t,\tau)$, where $\epsilon(\xi)$ denotes the dependence on the entire motion history. Furthermore, the nonlinear indicial theoretical formulation allows for the presence of aerodynamic bifurcations by splitting the integral, i.e., for example:

$$\begin{aligned} f(t) &= f(\epsilon(\xi);t,0) + \int_0^{\tau_c} \frac{d\epsilon}{d\tau}\tilde{f}(\epsilon(\xi);t,\tau)d\tau \\ &+ \Delta f^{CS}(t;\epsilon(\tau_c)) + \int_{\tau_c}^t \frac{d\epsilon}{d\tau}\tilde{f}(\epsilon(\xi);t,\tau)d\tau \end{aligned} \qquad (2)$$

where the nonlinear indicial function $\tilde{f}(\epsilon(\xi);t,\tau)$ is defined as the following Fréchet derivative:

$$\begin{aligned} \tilde{f}(\epsilon(\xi);t,\tau) &= \lim_{\Delta\epsilon\to 0}\frac{\Delta f(t)}{\Delta\epsilon} \\ &= \lim_{\Delta\epsilon\to 0}\left[\frac{f(\epsilon(\xi) + H(\xi-\tau)\Delta\epsilon) - f(\epsilon(\xi))}{\Delta\epsilon}\right] \end{aligned} \qquad (3)$$

and $\Delta f^{CS}(t;\epsilon(\tau_c))$ is the so-called jump response associated with crossing the bifurcation at time τ_c.

A critical state is defined as a transition from one equilibrium flow state to another (Ref. 11) and is often associated with a discontinuity in the static aerodynamic loads and/or their derivatives (Ref. 12). The associated transient response may be associated with large time lags and is referred to either as the critical-state response (CSR) or the jump response, $\Delta f^{CS}(t;\epsilon(\tau_c))$.

3. KERNEL RESPONSE IDENTIFICATION AND EXTRACTION

In previous studies, indicial and critical state responses have been determined either directly, as the difference between two aerodynamic responses, or by optimization/parameter identification methods (Ref. 13). An alternative to these methods was recently developed. This alternative scheme is tightly coupled to the present (nodal) implementation of nonlinear indicial theory and uses projection methods which can result in linear systems of equations. Preliminary results from the application of this method (referred to as SMS, see below) were given in Reference 1. A key advantage of this method is that it requires no prior assumptions about the functional form of the indicial or critical state responses and, most importantly, does not require that the maneuvers approximate steps. In the case where the maneuvers start from rest (start-up maneuvers), the determination of **n** indicial responses requires in principle that an equal number of independent maneuvers be performed. If **p** critical state responses must also be extracted, then a total of at least **n**+**p** maneuvers is required; however, this time the system of equations is **a priori** nonlinear, unless the location of the critical states is known.

The present section describes the SMS extraction method and introduces a second method, which is based on the concept of Singular Value Decomposition (SVD). A brief rationale for the introduction of both the SMS and SVD extraction methods is given first. This is followed by a description of the extraction algorithms. Results obtained using these algorithms are shown in Section 4.
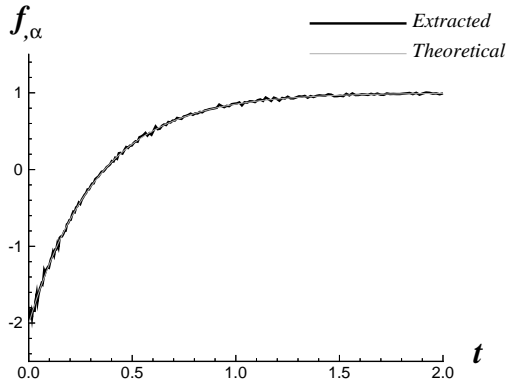

Fig. 1. Extracted Indicial Response Versus Theoretical Indicial Response. (Input data consisted of four monochromatic motions, at ω = 2.09, 4.18, 8.36, 14.66; time constant is τ = 0.33; SMS method with 200 points, 200 realizations).

Rationale

In the SMS method, indicial and/or critical state responses are represented as discrete data points (perhaps on the order of 200 points). When the motion is periodic, the matrices which naturally arise from the convolution problem, **Eq. (1)**, are Toeplitz matrices which happen to be rank-deficient. The Stochastic Matrix Solving (SMS) procedure was introduced in an attempt to desingularize these matrices through the introduction of random perturbations (see Theory section, below). This method was shown to yield accurate results on the basis of synthetic signals (Ref. 1) and it was later shown to be robust with respect to noise (Ref. 3).

A drawback of the SMS extraction method is that it is expensive, requiring hundreds, maybe thousands, of matrices to be formed. These performance issues, along with the lack of a proper mathematical foundation to explain the success of the SMS procedure, have prompted us to review the fundamentals of the identification and extraction scheme. Thus, two complementary ideas were investigated. The first one is the method of singular value decomposition. This method expands the solution onto the basis of eigenvectors, and truncates the expansion in such a manner that only the significant eigenvalues (those above the noise floor) are retained. The second improvement is to consider a judicious choice of efficient basis functions on which to expand the IR and CSR solutions.
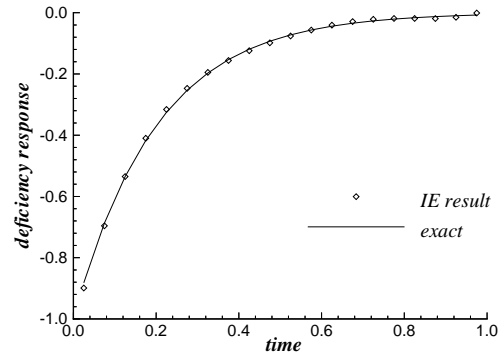

Fig. 2. Identification/Extraction Result Using Singular Value Decomposition. (Input data consisted of three monochromatic motions, at ω = $\pi/2$, π, and 2π; time constant is τ = 0.2; single realization).

Prior to presenting the theoretical description and the algorithm behind the two extraction methods, a preliminary result for the case of linear indicial theory is shown by way of illustration. **Figure 1** depicts the SMS-extracted indicial response f_α for a linear system whose known indicial response (dotted grey line) is a simple exponential. The indicial response was extracted from four pure-harmonic motions $\alpha(t)$ using 200 realizations of a 200×200 matrix. By contrast, **Figure 2** depicts the result of an SVD-based extraction (symbols) versus the theoretical exponential response (solid line). The linear system and data set used in **Figure 2** are different from those of **Figure 1**; thus, this

is not intended to be a direct comparison between the two methods. However, **Figure 2** (obtained using sinusoidal data at three forcing frequencies and uniformly-spaced unit pulse basis functions) is the result of a single matrix inversion.

Theory

In this section, we attempt to present the SVD and SMS extraction methods in a unified way, up to a point, and then stress where the methods differ in the final solution stage. A simplified version of the SMS equations is derived. These equations are then generalized to set up the SVD problem. It will also be apparent, in the process, that the SVD and SMS methods are not mutually exclusive, although their combination is beyond the scope of the present paper.

Let us begin with the task of extracting a single indicial response. In order to deal with finite-sized systems, it is preferable to solve for the deficiency response. (The deficiency response is the indicial response, minus its time-asymptotic value). This can always be done in practice, provided that the dynamic (i.e., total minus static) response is known. For simplicity, let us also consider a single-input, single-output system. Let α designate the input, and f designate the dynamic component of the output. If $\tilde{h}$ is the deficiency response of f with respect to α, then, according to linear indicial theory:

$$f(t) = \int^t \tilde{h}(\tau)\, \dot{\alpha}(t-\tau)\, d\tau \qquad (4)$$

(the lower bound of the integration is intentionally omitted, with the understanding that the integration proceeds backwards in time until $\tilde{h}(\tau) \approx 0$).

In the SMS method, we regard the deficiency response as being represented by the discrete samples of $\tilde{h}$, $\tilde{h}_j \equiv \tilde{h}(t_j)$, which are considered as unknowns which must be solved for.

This idea is generalized by considering the unknown deficiency response to be expanded in some basis function space:

$$\tilde{h}(t) = \sum_j x_j \xi_j(t) \qquad (5)$$

Thus, in the previously considered case, the coefficients x_j are the discrete samples $\tilde{h}_j$, and the basis functions $\xi_j(t)$ are unit-height, finite-width pulses which are uniquely defined, given an ordered sequence $t_0 < t_1 < \cdots < t_n$, e.g.:

$\xi_j(t) \equiv H(t-t_{j-1/2}) - H(t-t_{j+1/2})$. Combining **Eqs. (4)**

and **(5)** yields the following equation for $f(t)$:

$$f(t) = \sum_j x_j \int^t \xi_j(\tau)\, \dot{\alpha}(t-\tau)\, d\tau \qquad (6)$$

Equation (6) is regarded as a constraint which the x_j basis coefficients must satisfy at all times. Thus, in the SMS method, we must solve for n coefficients, x_1 through x_n, by constructing at least n independent realizations of **Eq. (6)** in order to solve for the x_j's. Each realization might be expressed as

$$f(t_i) = \sum_j x_j \int^{t_i} \xi_j(\tau)\, \dot{\alpha}(t_i-\tau)\, d\tau$$
$$or \qquad f_i = \sum_j x_j a_{ij} \qquad (7)$$

In principle, the coefficients a_{ij} can be calculated using any integration method, since the input $\alpha(t)$ is known, and so are the basis functions, $\xi_j(t)$. The main point is that, for each realization of **Eq. (6)**, one obtains a row of a matrix. Thus, the basic principle behind the common extraction procedure of both the SMS and SVD methods is that, through multiple instances of the hypothesized indicial model (the linear model of **Eq. (4)**, in this case), one ends up formulating a matrix problem of the type

$$AX = F \qquad (8)$$

where $A \equiv [a_{ij}]$ is the motion matrix, $F = [f_1, f_2, \cdots, f_n]^T$ is the data, and $X = [x_1, x_2, \cdots, x_n]^T$ is the solution vector.

Equation (8) is fundamental to the extraction method. The same equation is obtained, whether one is solving for 200 numerical samples of a deficiency response, or, say, three coefficients in a judiciously chosen basis function expansion (Jacobi polynomials and the like). Most importantly, the same fundamental equation can be obtained for nodal-based *nonlinear* indicial response (NIR) schemes. In this case, multiple indicial and critical-state responses must be simultaneously extracted (see below).

The main difference, then, between the SVD and SMS techniques, relates to *how to solve* **Eq. (8)**. Simply stated, the problem is this: the matrix A is, in general, singular. Note that this is not at all an unusual situation, as most inverse problems are, fundamentally, improperly posed. They require, therefore, the use of specialized techniques (Refs. 14,15) for solving discrete ill-posed equation systems.

The reason for which A is singular can be looked at in several ways. One of them is the nonuniqueness issue: there may be more than one indicial response that

- 4 -

reproduces the data. For example, it can be shown that, for harmonic motions, the rank of the motion matrix is two, regardless of matrix size. Mathematically, the improperly posed nature of the inverse problem follows from the well-known Riemann-Lebesgue lemma, which states that if the kernel oscillates rapidly, the integral goes to zero in the limit. Conversely, computing the kernel from the knowledge of the output $f(t)$ will tend to amplify any high frequency components of $f(t)$. This is the crux of the matter, since the measurements of $f(t)$ must be assumed to be <u>noisy</u> measurements. A second, related reason is simply that the right-hand side, F, simply may *not* satisfy the assumed nonlinear indicial model. The latter is a function, among other things, of the parameterization of the problem.

Both issues (lack of a unique solution, when it exists, or absence of an exact solution) are addressed by considering the solution to $AX = F$ in the least squares sense. In other words, we require that the solution vector X simultaneously satisfy a set of maneuvers or data sets $A^{(n)}X = F^{(n)}$ in an approximate sense. Such a condition is expressed in the usual manner, i.e., by minimizing the modeling error in the least squares sense, which results in the following matrix equation:

$$\text{or} \quad \begin{array}{c} \sum_n A^{T\,(n)}A^{(n)}X = \sum_n A^{T\,(n)}F^{(n)} \\ \\ MX = B \end{array} \quad (9)$$

where M is the least squares motion matrix and B is the least squares data vector.

Note that, depending on the motions available, the linear system, **Eq. (9)**, may still be stiff, and the challenge is to find a "good" solution to $MX = B$. Such a solution is obtained by different means in the SMS and SVD procedures. In the SVD procedure, one carries out a so-called pseudo-inversion of M, based on the eigenvalue spectrum of the matrix (see below). In the SMS procedure, we use a direct (L-U decomposition) solution procedure; however, M is first regularized by extending the least squares solution technique to perturbations on the basis functions themselves. The characteristics of each method will be described in greater detail below. Prior to doing this, however, we proceed with the generalization of **Eq. (7)** to the case of *nonlinear indicial theory*.

Let us first consider the case where the deficiency response at a given point in time can be expressed as a linear combination of the nodal deficiency responses:

$$\tilde{h}(t) = \sum_k c_k \tilde{h}_k(t)$$

The nodal responses $\tilde{h}_k$ are the unknowns, and the c_k's are the interpolation coefficients. They (the c_k's) are implicitly time-dependent, through the parameterization of the IR/CSR space (Ref. 16). If the nodal responses are now expanded in terms of a common set of basis functions ξ_j:

$$\tilde{h}_k(t) = \sum_j x_{jk} \xi_j(t)$$

the following constraint must hold for f at all times t_I:

$$f(t_I) = \sum_k \sum_j x_{jk} \int^{t_I} c_k \xi_j(\tau)\,\dot{\alpha}(t_I-\tau)\,d\tau \qquad (10)$$

By in-lining the x_{jk} array, **Eq. (10)** can be symbolically rewritten as

$$f_I = \sum_{J=1}^{k_{max} \times j_{max}} x_J a_{IJ} \qquad (11)$$

which is the analog of **Eq. (7)**. Note that x_J is now an extended vector containing the basis coefficients of all nodal responses, and the a_{IJ} coefficients differ from the a_{ij} integrals only in the sense that the interpolation coefficients c_k must be taken into account. Thus, by considering $k_{max} \times j_{max}$ independent realizations of **Eq. (11)**, one ends up formally with the same matrix system $AX = B$ as **Eq. (8)**.

Let us now consider the existence of a critical state response whose deficiency response (dynamic component) $\tilde{H}$ is expressed as a linear combination of nodal critical-state deficiency responses, $\tilde{H}_m$:

$$\tilde{H}(t) = \sum_m d_m \tilde{H}_m(t)$$

If the nodal critical-state responses are similarly expanded in terms of the same basis functions ξ_j:

$$\tilde{H}_m(t) = \sum_j z_{jm} \xi_j(t)$$

then, $f(t)$ at time t_I is expressed as

$$\begin{aligned} f(t_I) = & \sum_k \sum_j x_{jk} \int^{t_I} c_k \xi_j(\tau)\,\dot{\alpha}(t_I-\tau)\,d\tau \\ & + \sum_m \sum_j z_{jm} d_m \xi_j(t_I-t_{CS}) \end{aligned} \qquad (12)$$

It is implicitly assumed, in the adopted notation, that $\xi_j(t) = 0$ for $t < 0$. By in-lining the x_{jk} and z_{jm} arrays together, **Eq. (12)** can be symbolically rewritten as

$$f_I = \sum_{J=1}^{(k_{max}+m_{max})j_{max}} y_J \, a_{IJ} \qquad (13)$$

which, again, is analogous to **Eq. (7)**, provided that the extended vector y_J contains all (indicial and critical-state response) basis coefficients, and provided that the matrix term a_{IJ} assumes the proper form (integral or algebraic) and uses the appropriate interpolation coefficients. The generalization to multiple critical states (not shown) is straightforward.

In summary, if k_{max} designates the maximum number of indicial response nodes to be determined, and m_{max} is the maximum number of critical-state response nodes, then $(k_{max}+m_{max}) \times j_{max} = N$ independent instances of the nonlinear indicial formalism will result in an $N \times N$ linear system of simultaneous equations, $AX = B$.

Having established the generality of **Eq. (8)** and, therefore, of **Eq. (9)** (its least squares counterpart), we now address the differences between the SVD and SMS solution procedures. We begin with the essentials of the SVD method and conclude this theoretical section with a description of the current SMS implementation.

In the SVD method, the linear system $MX = B$ is solved by taking the pseudoinverse of M. This procedure is the topic of many texts (see, for instance, References 15 and 17). We do not attempt to repeat the theory but provide, instead, the essential idea in a simplified form. Recall that, if M is nonsingular and diagonalizable, its eigenvectors form an orthonormal set $\{u_i\}$ and the solution X can be expressed as the following linear combination of the u_i's

$$X = \sum_{i=1}^{N} \frac{1}{\lambda_i} <u_i, B> u_i$$

where λ_i are the eigenvalues and $<u_i, B>$ is the inner product of the u_i and B vectors.

If the matrix M is singular (has one or more null eigenvectors), then an approximate solution (the pseudoinverse) is obtained by retaining only those eigenvectors for which the associated eigenvalue is nonzero. Thus, if the eigenvalues are sorted and if P eigenvalues (λ_1 through λ_P) are nonzero, the pseudoinverse-based approximate solution is

$$X^* = \sum_{i=1}^{P} \frac{1}{\lambda_i} <u_i, B> u_i$$

Of course, in practice, one has to decide which of the eigenvalues are effectively considered to be zero. At present, the SVD method is implemented in such a way that the least squares matrix is formed using a number of motion matrices R which is equal to the number of data sets included in the training.

By contrast, the SMS method solves $MX = B$ directly, using a standard L-U decomposition technique. Experience has shown, however, that, if R is simply the number of maneuvers, then M is typically too ill-conditioned in order to solve for X (this is particularly true of harmonic motions). Thus, the SMS method *artificially* extends the available number of realizations for **Eq. (13)** by introducing stochastic perturbations in the matrix. These stochastic perturbations are not simply random numbers: they are perturbations <u>of</u> the basis functions themselves. In the present implementation, the widths of the unit pulses are changed each time a new row of the motion matrix is formed. This assures a virtually limitless supply of equations (realizations) and, in the final analysis, desingularizes the matrix M. The key step, implied by this analysis, is that the perturbed basis functions are, in some sense, sufficiently similar to each other that each solution component x_i is effectively the coefficient for a "representative" basis function ξ_i. This is done by choosing initially a nominal sequence $t_0 < t_1 < \cdots < t_n$ and perturbing this sequence with a zero-mean stochastic process. Each row formed then represents a slightly different expression (realization) of the same instance (a nonlinear indicial constraint).

The number of formed motion matrices in the SMS method is typically $R = (k_{max}+m_{max}) \times r$, where r is the number of random perturbations of the M matrix. Therefore, the SMS method can be expensive. For example, if we are simultaneously solving for 10 responses, each characterized by 100 samples, and if the number of random perturbations needed to converge is 100, then the method will assemble a total of 100 motion matrices, each 1000×1000 in size. These numbers can be compared to the relative efficiency of the SVD method. For example, if 10 responses were to be extracted using SVD from 15 data sets, and if each response is represented by four terms of an appropriately chosen function basis (e.g., Laguerre polynomials), then the motion matrices are only 40×40 in size, and only 15 such matrices would need to be formed.

In principle, the SVD and SMS methods are not mutually exclusive. For instance, the performance of the SMS method might be improved with a more efficient choice of basis functions. In the case where the basis functions are Laguerre polynomials, for example, the weight function multiplying each polynomial is a decaying exponential. It is possible that, by changing slightly the time constant of the exponential from realization to realization, one might achieve an effect similar to the randomization (desingularization) previously achieved on the finite-width pulse function basis. Conversely, the finite-width pulse function basis ought to be a valid choice for SVD.

However, early tests of this idea have not proved successful. As a result of these early tests, we have focussed our efforts on finding basis functions which exhibit the proper physical behavior for representing deficiency responses (i.e., in particular, a decay to zero at large times). Several families of orthogonal polynomials were considered. Among the possibilities (Ref. 18) are: Jacobi polynomials (finite support), and Laguerre and Generalized Laguerre polynomials (both with semi-infinite support).

4. RESULTS

As previously discussed, the task of extracting indicial and critical-state responses from unsteady data can be reduced to a linear inverse problem. The ill-posed nature of this inverse problem leads to the use of specialized solution techniques and places extra requirements in terms of method validation. In other words, since more than one kernel of responses can reproduce the training data, it is critical that the method be tested against systems where the indicial and critical-state responses are known.

For this reason, the extraction method has undergone considerable scrutiny, using a variety of synthetic data. Synthetic data are data constructed using a nonlinear indicial model with known indicial and critical-state responses. In this manner, one can assess directly the accuracy of the extraction procedure, including the effects of noise and other imperfections, prior to proceeding with real data, where the "answer" is not known. Unless otherwise specified, all of the results presented here pertain to the SVD extraction method.

Basic Demonstration

The basic operation of the extraction technique can be illustrated by means of the following example. In this example, the system being considered is nonlinear, and the right-hand side is nonexact. The artificially constructed data were based on a single parameter (equal to the degree of freedom, α), piecewise linear system consisting of two partitions ($\alpha < 0$ and $\alpha \geq 0$) and one critical state at $\alpha = 0$. A single deficiency response characterizes the "left" partition ($\alpha < 0$): $DR_{LEFT}(t) = -\exp(-5t)$. Likewise, the right-hand side ($\alpha \geq 0$) deficiency response is $DR_{RIGHT}(t) = -2\exp(-3t)$. In addition, the dynamic component of the critical-state response crossed in the normal direction (*LEFT* to *RIGHT*) is given by $CSDR(t) = \exp(-2t)$.

The training data consisted of four harmonic motions and one ramp motion. Two types of basis functions were used for the extraction: exponentials and Laguerre polynomials. The exponential basis functions were designed to form a complete set ($\xi_j(t) = \exp(-jt)$, $j = 1,..,8$). By contrast, the Laguerre polynomial basis (which used eight terms also) did

not form a complete set. In other words, the theoretical (underlying) deficiency responses, DR_{LEFT}, DR_{RIGHT}, and $CSDR$, cannot be represented exactly using the Laguerre polynomial basis.
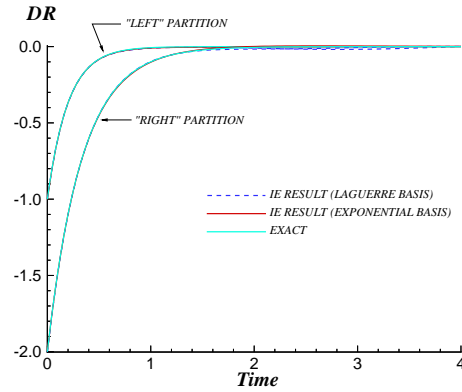

Fig. 3. Effect of Function Basis on Indicial Response Node Extraction.

The results of the extraction are shown in **Figures 3** and **4**. **Figure 3** compares the deficiency responses DR_{LEFT} and DR_{RIGHT} extracted using either set of basis functions, to the exact theoretical values. A similar comparison is given in **Figure 4** for the dynamic portion of the extracted critical-state response.
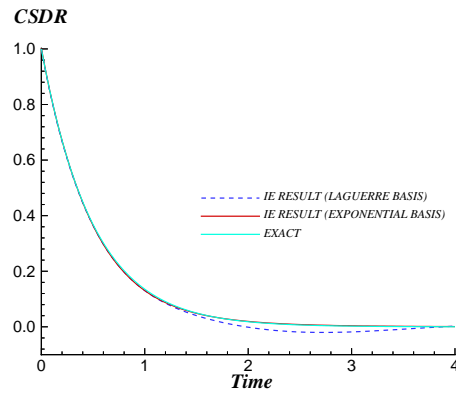

Fig. 4. Effect of Function Basis on Critical-State Response Node Extraction.

Close examination of these curves reveals that the error, defined as $\dfrac{\max(|DR_{exact} - DR_{calc}|)}{\max(|DR_{exact}|)}$, calculated over all three extracted responses, is on the order of one percent in the case of the exponential basis functions, and approximately three percent when using the Laguerre polynomials.

The above results show that the underlying extraction theory works and that good results can be obtained, even if the basis functions are not optimal. The results of **Figures 3** and **4** demonstrate that the method is capable of extracting the same set of IR/CSR nodes using different basis functions.

Sensitivity to Noise

The goal of the present section is to illustrate the robustness of the extraction method by carrying out extractions with various amounts of noise on the training data. Two examples are considered. The first is based on synthetic data. The second corresponds to the 65-degree delta wing example.

Synthetic Data. An important exercise in the validation of the method is to demonstrate convergence with respect to noise. The question that must be answered is this, "How sensitive are the extraction results to the presence of noise in the data?" To answer this question, consider the simple case of a linear indicial response (i.e., a single node) extraction. By construction, the theoretical deficiency response for this system is chosen to be a five-term linear combination of Laguerre polynomials. The five basis functions used in the extraction were chosen to form a complete set, and the training data were composed of harmonic responses of various frequencies.
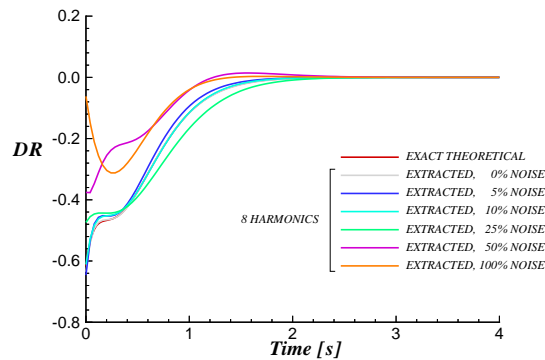
Fig. 5. Sensitivity of Single Node Extraction to Data Noise Amplitude.

A number of tests were then conducted in which the synthetic data were contaminated by adding controlled amounts of noise. The total noise level, expressed as the root mean square error percentage with respect to the amplitude of the zero-noise response, was varied in increments between 0% and 100%. In addition, the frequency content of the noise component could be controlled by specifying the number of harmonics to be retained, with respect to the fundamental frequency of the data.

Figure 5 shows the effect of noise amplitude for a given number of retained harmonics. In this figure, the exact theoretical indicial response and that extracted with zero added noise are practically indistinguishable from one another, as one would expect. Small deviations from ideal behavior are observed at noise levels of five and ten percent. The "errors" only become large when the noise level reaches 50% and above. The term "error" is, of course, a misnomer, since the data are indeed altered by the presence of the noise and there is no telling, under these conditions, what the indicial response ought to be. Indeed, it was verified that the extracted indicial responses are a better "fit" to the noisy data than the theoretical response.

A separate, related exercise is to keep the noise level constant and to vary the frequency content of the noise (referred hereafter as bandwidth). One such example (for 25% noise level) is given in **Figure 6**. The interpretation of these results is less clear, since the behavior with respect to the number of retained harmonics is not monotonic. As previously mentioned, the presence of noise does alter the data, causing the extracted responses to differ, depending on the frequency content. It is interesting to notice, however, that, even at a 25% noise level, the extracted responses exhibit a qualitatively similar behavior for a range of bandwidths.
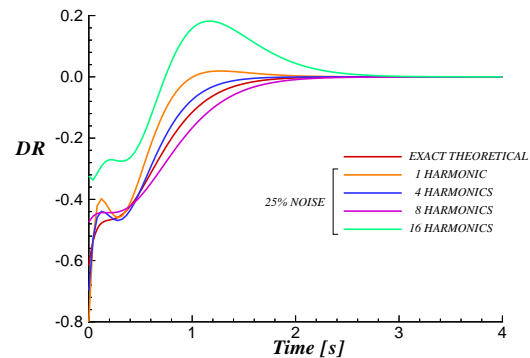

Fig. 6. Effect of Data Noise Frequency Content on Single Node Extraction.

The results shown in **Figure 5** indicate smooth convergence towards the theoretical response. Taken together, **Figures 5** and **6** also give a sense of the relative robustness of the extraction method with respect to noise. While this is a desirable property in general, robustness with respect to noise is particularly important here, in view of the improperly posed nature of the extraction problem (see Section 3).

65-Degree Delta Wing Data. For real data, the indicial and critical-state responses are not known. Thus, it is not possible to assess the accuracy of the extraction directly.

One method is to use the extracted responses to repredict the data and calculate the error metrics. This approach, however, only tests the method's ability to 'fit' the data with reasonably low error: it is a necessary (but not sufficient) condition. Another (more demanding) approach is to compare the extracted responses to each other and hope to establish some form of convergence, as the noise level is gradually reduced.

As previously mentioned, with different noise characteristics (controlled here by the amount of filtering), the data are, effectively, different, and there is no reason to suspect *a priori* that the indicial or critical-state responses should resemble each other (see, for example, **Figure 6**). However, this is a reasonable expectation when the noise level approaches zero.

This hypothesis was tested on the dynamic rolling moment data of a 65-degree delta wing in what was previously referred to (Ref. 19) as Region I (-4° < ϕ < 5°) and Region II (5° < ϕ < 8.5°) of the roll angle range (see Ref. 9 for further details). These data are part of a comprehensive database of unsteady aerodynamic responses acquired as a result of a joint program between the U.S. Air Force Research Laboratory (formerly USAF/WL) and the Canadian Institute for Aerospace Research (IAR). For all of the tests mentioned here, the delta wing is undergoing forced rolling motions at a body axis angle with respect to the freestream of 30 degrees. The freestream Mach number is three tenths.
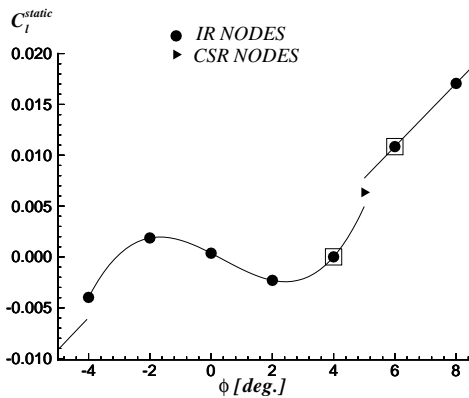

Fig. 7 Location of IR and CSR Nodes in Regions I and II of the Static Rolling Moment Curve with Respect to Roll Angle.

The employed methodology was as follows. Four separate training data sets were generated, each with a different level of harmonic filtering: unfiltered data, 64-harmonic data, 32-harmonic data, and 16-harmonic data (a more precise definition of these terms is provided in Refs. 9,16). Both periodic and ramp data were used in the training data.

The IR and CSR nodes were parameterized by the instantaneous roll angle and sign of roll rate. A summary representation of the IR/CSR node locations with respect to ϕ is given in **Figure 7**. A total of 10 IR nodes were extracted in Region I, four IR nodes in Region II, and two CSR nodes between Regions I and II (one for positive roll rate and one for negative roll rate).

The most sensitive region for the extraction is in the immediate vicinity of the critical state. Thus, the following figures focus on the variations of extracted IR and CSR nodes at ϕ = 4° (the right-most node pair of Region I), ϕ = 6° (the left-most node pair of Region II), and at ϕ_{CS} = 5°. The two IR nodes in question are indicated in **Figure 7** using a square symbol. **Figures 8** and **9** provide comparisons of the extracted indicial responses at a ϕ = 4° (Region I) and ϕ = 6° (Region II). A similar comparison for one of the CSR nodes is given in **Figure 10**.
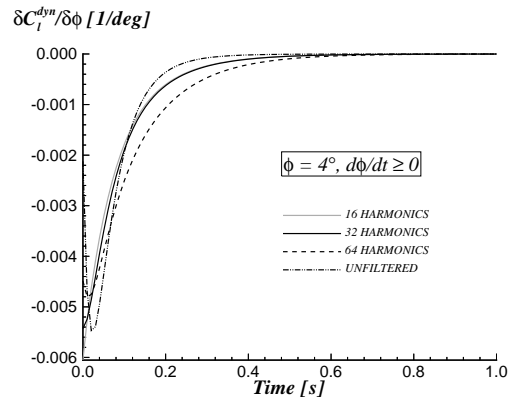

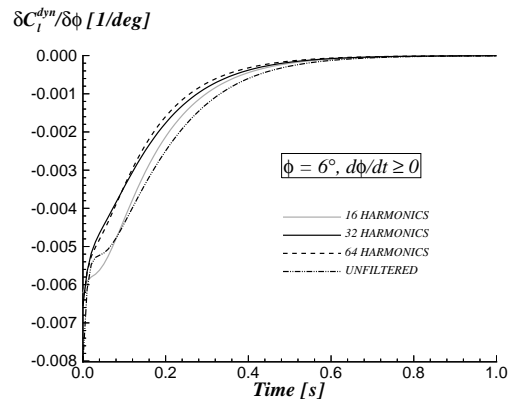**Fig. 8** Effect of Filtering on the Extracted Indicial Responses at ϕ = 4°, Positive Roll Rate.

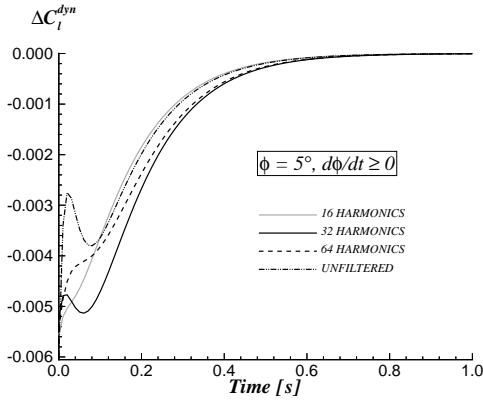**Fig. 9** Effect of Filtering on the Extracted Indicial Responses at ϕ = 6°, Positive Roll Rate.

Fig. 10 Effect of Filtering on the Extracted Critical-state Responses at $\phi = 5°$, Positive Roll Rate.

The results shown in **Figures 8**, **9**, and **10** are fairly typical. They illustrate two main points. The first is the fact that the responses converge as the noise is reduced (i.e., as filtering is increased). The second is the observation that convergence is most difficult to attain on the critical-state responses.

Convergence

Perhaps the most important property of the extraction method is its ability to accurately characterize the underlying system, as opposed to simply fitting the data. This must be verified by checking that the theoretical model can reproduce novel maneuvers, i.e., maneuvers that were not included in the training data used for extraction (examples of novel maneuver predictions are given in Ref. 9). A related exercise consists of verifying that the extracted responses themselves do not change significantly with incremental enrichments of the training data set.

The reasoning is as follows. If, as more data are included in the training, the extracted responses "jump around," then it is likely that the extraction process is merely fitting the data or, alternatively, that the new pieces of information brought on by the new data are significant enough to change the most likely kernel. If, on the other hand, the addition of new maneuvers to the training data set does not produce large changes in the results, then the method is said to be convergent.

This convergence property will be illustrated below on the example of the rolling moment of the 65-degree delta wing at a body axis angle with respect to the freestream of 30 degrees and a Mach number of three-tenths. The extraction of the Region I indicial response nodes will be considered first. This will be followed by the IR and CSR extraction in Region II.

The total number of available maneuvers in Region I is 18 (15 harmonic maneuvers and three ramp-and-hold rolling

motions). Instead of carrying out the ten-node extraction of Region I using all 18 maneuvers, randomly chosen groups of maneuvers are used for the extraction. The first training set consists of three randomly chosen maneuvers. The second set consists of those same three maneuvers, plus three more (randomly picked among the remaining 15). The third set consists of the previous six, plus three additional maneuvers (randomly picked among the remaining 12), and so on.

Figure 11 shows the evolution of the extracted deficiency response at $\phi = 4°$, $d\phi/dt > 0$, as a function of the training data set. After nine maneuvers, the extracted indicial response is seen to converge smoothly towards its value when using the full data set. Similar results (not shown) are obtained for the other nine indicial response nodes.
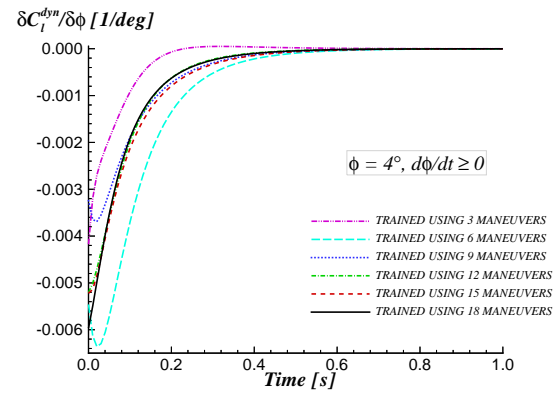

Fig. 11 Convergence of the Extracted Indicial Response, $\phi = 4°$, Positive Roll Rate.

The convergence property is also evident in the error metrics (**Figure 12**), which indicate a gradual reduction of the prediction error as more maneuvers are included in the training data.
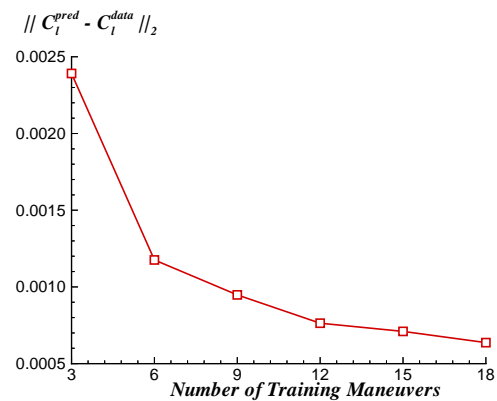

Fig. 12 Error Metrics for Region I, as a Function of Training Data Set Enrichment.

The error metrics are computed as follows. For a given training data set, ten IR nodes are extracted. These extracted nodes are used, in turn, to predict all 18 Region I maneuvers. The error is the norm-2 or rms error between the data and the prediction, computed over all 18 maneuvers.
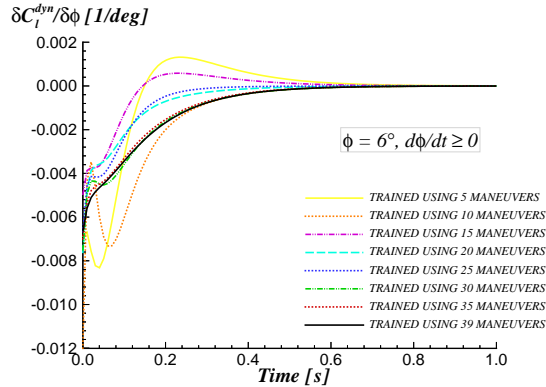
$\delta C_l^{dyn}/\delta\phi \ [1/deg]$

$\phi = 6°, \ d\phi/dt \geq 0$

TRAINED USING 5 MANEUVERS
TRAINED USING 10 MANEUVERS
TRAINED USING 15 MANEUVERS
TRAINED USING 20 MANEUVERS
TRAINED USING 25 MANEUVERS
TRAINED USING 30 MANEUVERS
TRAINED USING 35 MANEUVERS
TRAINED USING 39 MANEUVERS

Time [s]

Fig. 13 Convergence of the Extracted Indicial Response, $\phi = 6°$, Positive Roll Rate.

ΔC_l^{dyn}

$\phi_{CS} = 5°, \ d\phi/dt \geq 0$

TRAINED USING 5 MANEUVERS
TRAINED USING 10 MANEUVERS
TRAINED USING 15 MANEUVERS
TRAINED USING 20 MANEUVERS
TRAINED USING 25 MANEUVERS
TRAINED USING 30 MANEUVERS
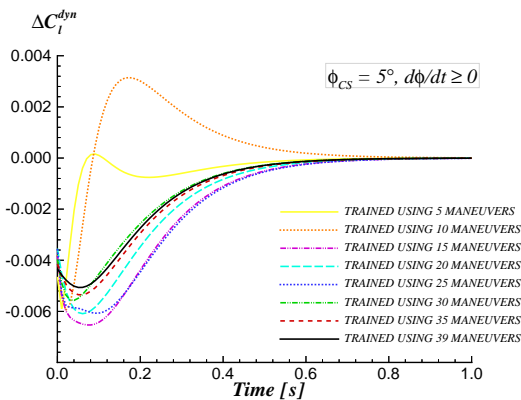TRAINED USING 35 MANEUVERS
TRAINED USING 39 MANEUVERS

Time [s]

Fig. 14 Convergence of the Extracted Critical-state Response, $\phi_{CS} = 5°$, Positive Roll Rate.

A similar procedure is used for Region II. There are no maneuvers in the database that span Region II alone. Thus, Regions I and II must be considered together. The total number of training maneuvers spanning simultaneously Regions I and II is 39, of which 20 are harmonic motions and 19 are ramp-and-hold. Once again, instead of carrying out the six-node extraction (four IR nodes of Region II, plus two CSR nodes) using all 39 maneuvers, randomly chosen groups of maneuvers are used for the extraction. The first training set consists of five randomly chosen maneuvers. The second set consists of those same five maneuvers, plus five more (randomly picked among the remaining 34). The third set consists of the previous ten, plus five additional maneuvers (randomly picked among the remaining 29), and so on.

Figures 13 and **14** illustrate, respectively, the convergence of the $\phi = 6°$, $d\phi/dt > 0$, indicial response node and that of the positive roll rate critical-state response node. After 25 maneuvers, the extracted indicial response is seen to converge smoothly towards its value when using the full data set. Similar conclusions are reached for the critical-state response (**Figure 14**), although the convergence rate is somewhat slower. It is also interesting to notice that one can get a fairly good idea of the time constants involved using relatively few maneuvers.

Once again, the convergence property is also evident in the error metrics (**Figure 15**), which indicate a gradual reduction of the prediction error as more maneuvers are included in the training data set.
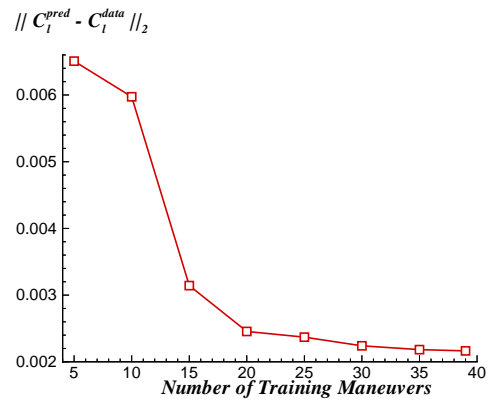
$|| \ C_l^{pred} - C_l^{data} \ ||_2$

Number of Training Maneuvers

Fig. 15 Error Metrics for Region II, as a Function of Training Data Set Enrichment.

The convergence property illustrated in **Figures 11-15** is evidence that the extraction method does indeed identify the system's kernel of indicial and critical-state responses.

Application to the 65–Degree Delta Wing

Having demonstrated the basic properties of the extraction algorithm, this Results section is concluded with the presentation of some of the extracted indicial and critical state indicial responses for the rolling moment response of the 65-degree delta wing (see **Figures 16** and **17**).

As previously mentioned, the 65-degree delta wing database was collected as part of a joint AFRL/IAR program to study high angle of attack vortical flow. As a result of this program, a wealth of unsteady aerodynamic responses are available for a variety of motions and flow conditions. Therefore, the 65–degree delta wing database is an ideal test bed for the application of nonlinear indicial response models. Although the database includes other Mach numbers (M) and body axis angles (σ) with respect to the freestream, the present calculations are limited to the M = 0.3, σ = 30° subcase. The maneuvers under consideration are all forced rolling motions $\phi(t)$. They

include harmonic motions of various mean angle, amplitude and frequency, and ramp-and-hold motions of various rates and initial and final roll angles.
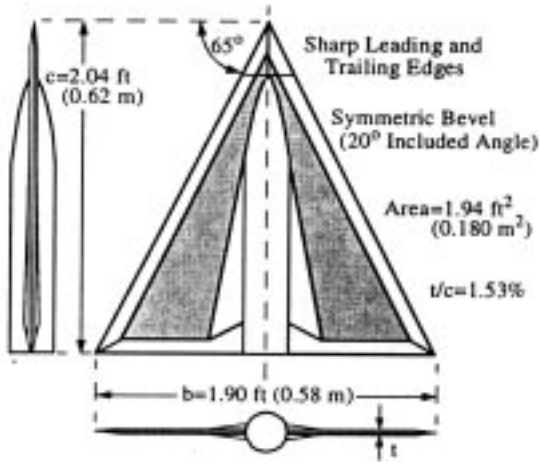

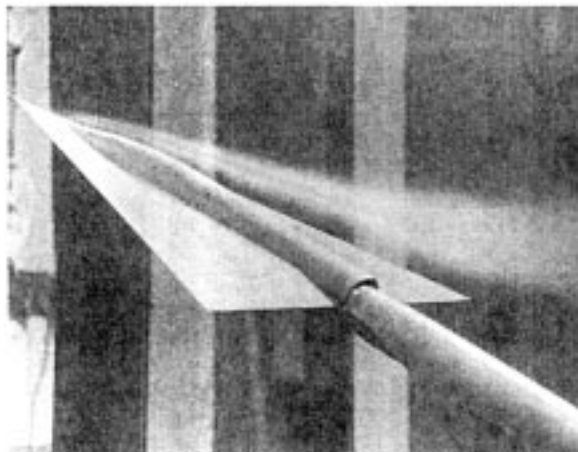**Fig. 16**   Delta Wing Model Geometry (from Ref. 13).

Fig. 17   Leeward Leading-Edge Vortex Burst at $\phi = -5°$ (from Ref. 12).

Aside from the wealth of unsteady aerodynamic data available, the case of the rolling 65-degree wing at high angles of attack is a challenging one, because it incorporates complex flow physics and flow state transitions having to do with changes in the topology of the vortical flowfield. Another benefit of using this database is that the physics of the flowfield are reasonably well-understood and the characteristics of this flow are well-documented (Refs. 11-13,19-21).

The description of the nonlinear indicial model and the results of the extraction on this database for C_l, C_m and C_N are the topic of a companion paper, Reference 9. A sample of the raw extraction results is given here for completeness.

Indicial Responses. **Figures 18**, **19**, and **20** depict the extracted deficiency responses corresponding, respectively, to the nodal locations $\phi = 0°$, $\phi = 4°$, and $\phi = 8°$. Each figure depicts three responses: the extracted response for positive roll rate, the extracted response for negative roll rate, and the deficiency response corresponding to Myatt's NIR model (Refs. 13,19) for the same configuration, which is included for reference.

Differences can be observed at $\phi = 0°$ and $\phi = 8°$ between the time constants for positive roll rate and negative roll rate. It is also interesting to notice, for these cases, that the deficiency response corresponding to Myatt's model appears to lie somewhere in between the positive and negative roll rate responses. This is, perhaps, not surprising, since, in Myatt's model, the indicial responses are parameterized by roll angle only, irrespective of roll rate. At $\phi = 4°$ the differences between positive and negative roll rates are reduced and, correspondingly, good agreement is found with Myatt's response.
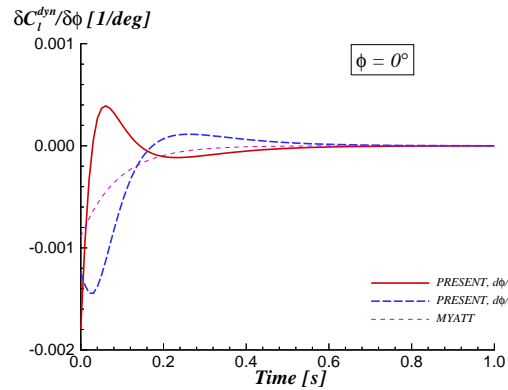

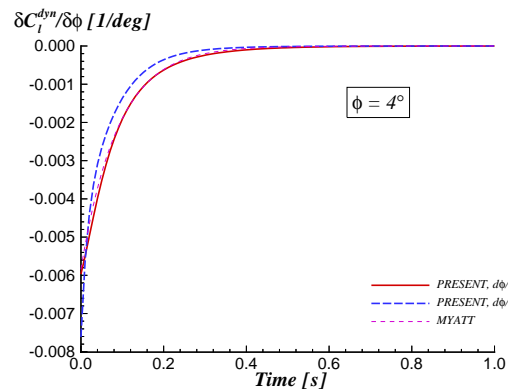**Fig. 18**   Extracted Rolling Moment Deficiency Responses at $\phi = 0°$.

Fig. 19   Extracted Rolling Moment Deficiency Responses at $\phi = 4°$.

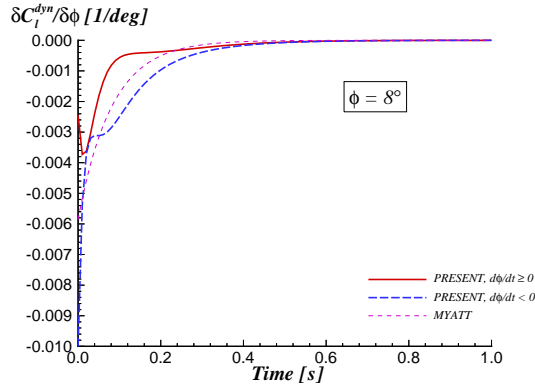**Fig. 20** Extracted Rolling Moment Deficiency Responses at $\phi = 8°$.

For comparison purposes, previous results obtained using the SMS extraction technique are shown in **Figure 21**. These results exhibit a lesser sensitivity to roll rate than the SVD-based extraction shown above. This question is still under investigation.
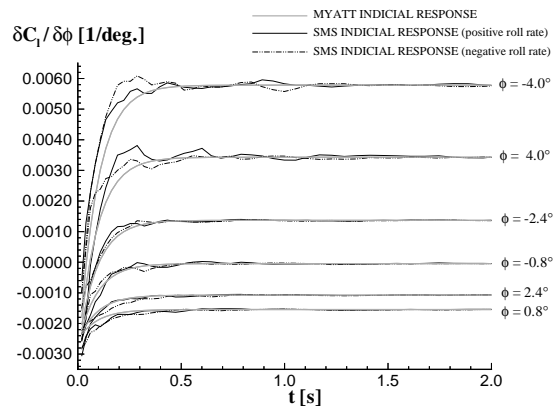

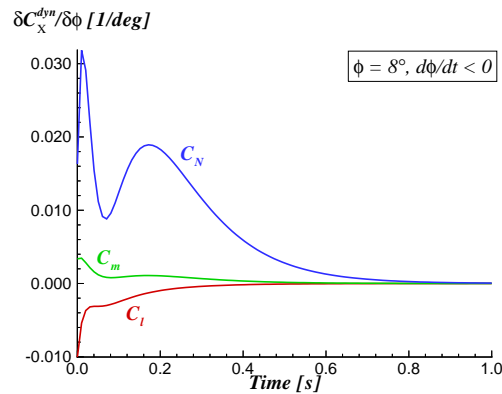**Fig. 21.** Extracted Indicial Responses Using SMS, $N_\phi = 6$.

Fig. 22 Comparison of Extracted Deficiency Responses for C_l, C_m, and C_N at $\phi = 8°$, $d\phi/dt < 0$.

SVD-based extractions have also been carried out for the pitching moment and normal force coefficients, although these cannot be compared against Myatt's model (which is for C_l only). For reference, **Figure 22** shows the extracted deficiency responses for C_l, C_m, and C_N at $\phi = 8°$ for negative roll rate. Note that the variety of shapes and apparent time constants is obtained with the same set of basis functions.

Critical-State Responses. An example of the extracted dynamic component of the critical-state response is shown in **Figure 23**, depicting the dynamic jump response incurred when the wing rolls from Region I to Region II. This transition occurs when the point of vortex breakdown on the windward side of the wing crosses the trailing edge on its way towards the apex (Reference 12).
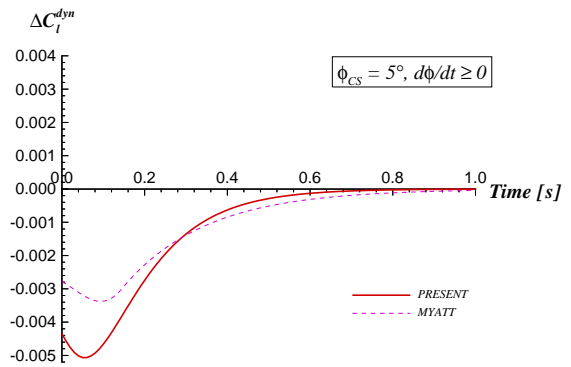

Fig. 23 Extracted Critical-state Response at $\phi_{CS} = 5°$, Positive Roll Rate.

Note that, while the time constants appear similar between the extracted critical-state response and that of the Myatt model, the latter is believed to be more accurate because the initial value of the total response (once the quasi-static value of the jump is added back) starts at zero, consistent with experimental observation. On the other hand, there is no such constraint in the current implementation of the extraction method. The parameter identification scheme used by Myatt (Refs. 13,19) assumes an exponential form for the lag of the vortical component of the static rolling moment. The present extraction scheme assumes a basis function representation using eight exponentials for the total dynamic component of the response. Most importantly, Myatt's identification of the critical-state responses is based on the analysis of ramp-and-hold maneuvers in the vicinity of critical states, resulting in a good correlation with the experimental data. By contrast, in the present method the extraction of critical states is the result of a global solution scheme involving all training maneuvers considered and the same basis function expansion as the indicial responses.

6. SUMMARY

The accuracy of indicial models depends on having access to the nonlinear indicial responses and critical-state responses of the system being modeled. The present paper describes a new extraction method which allows the identification of indicial and critical-state responses from experimental data, including harmonic data. The characteristics of the method are described, and its properties are illustrated using synthetic data cases, for which the "answer" (the underlying kernel of indicial and critical-state responses) is known. The identification procedure is then applied to a subset of the Air Force Research Laboratory / Canadian Institute for Aerospace Research 65-degree sweep delta wing database. The extraction method is shown to be robust with respect to noise and is also shown to be convergent, in the sense that nodes extracted from partial data sets converge towards the full-extraction set indicial and crtical-state responses.

ACKNOWLEDGMENT

REFERENCES

1   Reisenthel, P. H.: Development of a Nonlinear Indicial Model Using Response Functions Generated by a Neural Network, AIAA Paper 97-0337, Jan. 1997.

2   McKeehen, P. D., Myatt, J. H., Grismer, D. S. and Buffington, J. M.: Simulation of a Tailless Aircraft Using Nonlinear Indicial Response Aerodynamic Modeling Methods, AIAA Paper 97-3790, 1997.

3   Reisenthel, P. H., Bettencourt, M. T., Myatt, J. H., and Grismer, D. S.: A Nonlinear Indicial Prediction Tool for Unsteady Aerodynamic Modeling, AIAA Paper 98–4350, Aug. 1998.

4   Tobak, M., Chapman, G. T., and Schiff, L. B.: Mathematical Modeling of the Aerodynamic Characteristics in Flight Dynamics, NASA TM 85880, 1984.

5   Tobak, M. and Chapman, G. T.: Nonlinear Problems in Flight Dynamics Involving Aerodynamic Bifurcations, NASA TM 86706, 1985.

6   Reisenthel, P. H.: Novel Application of Nonlinear Indicial Theory For Simulation and Design of Maneuvering Fighter Aircraft, WL-TR-95-3094, Dec. 1995.

7   Reisenthel, P. H.: Development of a Nonlinear Indicial Model For Maneuvering Fighter Aircraft, AIAA Paper No. 96-0896, Jan. 1996.

8   Reisenthel, P. H.: Application of Nonlinear Indicial Modeling to the Prediction of a Dynamically Stalling Wing, AIAA Paper No. 96-2493, Jun. 1996.

9   Reisenthel. P. H. and Bettencourt, M. T.: Data-based Aerodynamic Modeling Using Nonlinear Indicial Theory, AIAA Paper 99-0763, Jan. 1999.

10   Nixon, D.: "Alternative Methods for Modeling Unsteady Transonic Flows," *Unsteady Transonic Aerodynamics*, Vol. 120 of Progress in Astronautics and Aeronautics, Ed. by D. Nixon, AIAA, 1989.

11   Jenkins, J. E., Myatt, J. H., and Hanff, E. S.: "Body-Axis Rolling Motion Critical States of a 65-Degree Delta Wing," *J. Aircraft*, Vol. 33, No. 2, 1996, pp. 268-278.

12   Jobe, C. E., Hsia, A. H., Jenkins, J. E., and Addington, G. A.: "Critical States and Flow Structure on a 65-Deg Delta Wing," *J. Aircraft*, Vol. 33, No. 2, 1996, pp. 347-352.

13   Myatt, J. H.: Modeling the Rolling Moment on the 65-Degree Delta Wing for Rolling Motions at High Angle of Attack, Ph.D. dissertation, Department of Aeronautics and Astronautics, Stanford University, Apr. 1997.

14   Chadran, K., Colton, D., Päivärinta, L., and Rundell, W.: *An Introduction to Inverse Scattering and Inverse Spectral Problems*, SIAM, Philadelphia, PA, 1997.

15   Hansen, P. C.: *Rank-Deficient and Discrete Ill-Posed Problems*, SIAM, Philadelphia, PA, 1998.

16   Reisenthel, P. H. and Bettencourt, M. T.: Development of a Nonlinear Indicial Prediction System for Unsteady Aerodynamic Modeling, AFRL-VA-WP-TR-1998-3036, Jan. 1999.

17   Tikhonov, A.N., Goncharsky, A. V., Stepanov, V. V., and Yagola, A. G.: **Numerical Methods for the Solution of Ill-Posed Problems**, Mathematics and Its Applications series, Vol. 328, Kluwer Academic Publishers, Dordrecht, The Netherlands, 1995.

18   Abramowitz, M. and Stegun, I. A.: **Handbook of Mathematical Functions**, Dover Publications, New York, NY, 1972.

19   Myatt, J. H.: Modeling the Rolling 65-Degree Delta Wing with Critical State Encounters, AIAA 97-3646, Aug. 1997.

20   Jenkins, J. E. and Myatt, J. H.: Modeling Nonlinear Aerodynamic Loads for Aircraft Stability and Control Analysis, AGARD Report 789, Feb. 1993, pp. 13/1-13/10.

21   Grismer, D. S. and Jenkins, J. E.: "Critical-State Transients for a Rolling 65° Delta Wing," *J. Aircraft*, Vol. 34, No. 3, May-Jun. 1997, pp. 380-386.